Arch. Metall. Mater., Vol. 61 (2016), No 1, p. 169–176

DOI: 10.1515/amm-2016-0030

J. KOZIEŁ*, L. BŁAŻ*,#, G. WŁOCH*, J. SOBOTA*, P. LOBRY*

PRECIPITATION PROCESSES DURING NON-ISOTHERMAL AGEING OF FINE-GRAINED 2024 ALLOY

Mechanical alloying and powder metallurgy procedures were used to manufacture very fine-grained bulk material made from chips of the 2024 aluminum alloy. Studies of solution treatment and precipitation hardening of as-received material were based on differential scanning calorimetry (DSC) tests and TEM/STEM/EDX structural observations. Structural observations complemented by literature data lead to the conclusion that in the case of highly refined structure of commercial 2024 alloys prepared by severe plastic deformation, typical multi-step G-P-B →θ'' →θ' →θ precipitation mechanism accompanied with G-P-B →S'' →S' →S precipitation sequences result in skipping the formation of metastable phases and direct growth of the stable phases. Exothermic effects on DSC characteristics, which are reported for precipitation sequences in commercial materials, were found to be reduced with increased milling time. Moreover, prolonged milling of 2024 chips was found to shift the exothermic peak to lower temperature with respect to the material produced by means of common metallurgy methods. This effect was concluded to result from preferred heterogeneous nucleation of particles at subboundaries and grain boundaries, enhanced by the boundary diffusion in highly refined structures.

Transmission electron microscopy and diffraction pattern analysis revealed the development of very fine Al_4C_3 particles that grow due to the chemical reaction between the Al matrix and graphite flakes introduced as a process control agent during the preliminary milling of chips. Al_4C_3 nano-particles are formed at high temperatures, i.e. during hot extrusion and the subsequent solution treatment of the samples. Highly refined insoluble particles such as aluminum carbide particles and aluminum oxides were found to retard recrystallization and reduce recovery processes during solution treatment of preliminarily milled materials. Therefore, the as-extruded material composed of a milled part and chip residuals retained its initial bimodal structure in spite of solution heat treatment procedures. This points to a high structural stability of the investigated materials, which is commonly required for new technologies of high-strength Al-based materials production.

Keywords: AA2024 alloy, scrap metal milling, structure refining, powder metallurgy, precipitation hardening.

1. Introduction

High mechanical properties of AA2000 series aluminum alloys can be attained via precipitation hardening, which depends on the composition of the material, heat treatment conditions, and processing procedures. The basic alloying elements used in technological practice to strengthen these alloys include copper, magnesium and silicon; zinc, manganese, vanadium, titanium and iron, on other hand, are micro-additives or impurities introduced from scrap metal commonly used in metallurgical procedures. Complex precipitation sequences in aged AA2000 series alloys are particularly affected by the Cu/Mg content ratio. According to literature data, the precipitation of at least five phases, marked as θ (Al_2Cu), S (Al_2CuMg), Si, β (Mg_2Si) and Q, is observed [1, 2, 3].

A Cu:Mg atomic ratio of ~1:1 leads to the hardening effect related to the presence of metastable phases that precede the formation of the S phase (rhombohedral, Al_2CuMg). At a relatively high Cu:Mg atomic ratio, the θ-phase (tetragonal, Al_2Cu) is also observed in addition to S-phase particles [3, 4]. The precipitation of both θ-type and S-type particles is preceded by Guinier-Preston-Bagaryatsky (G-P-B) zones; these zones are followed by the development of metastable phases. According to numerous reports, solid solution (SS) decomposition of Al-Cu alloys aged at low temperatures is accompanied by the sequence SS→G-P-B→θ''→θ'→θ (Al_2Cu) [4, 5]. However, relatively low Cu:Mg ratios lead to the precipitation of SS→G-P-B→S'' →S' →S (Al_2CuMg) sequences [1, 6, 7]. In the case of intermediate Cu:Mg ratios, the two sequences can contribute to age hardening processes [2, 3, 8]. The morphology of metastable θ'' and θ' particles is very similar to that of S'' and S' particles; therefore, an identification of the particles requires careful diffraction analysis using transmission electron microscopy (TEM) and X-ray diffraction (XRD) methods.

Precipitation sequences are often analyzed using differential scanning calorimetry (DSC) tests. Solid solution decomposition and phase precipitation reactions in DSC are studied at an increasing temperature, which may lead to conclusions on precipitation processes that are somewhat different than those based on experiments performed at constant ageing temperatures. Overlapping precipitation of θ'-type and S'-type particles, which often form in precipitation-hardened 2024 alloys containing Mg additions, may be assumed to be the underlying cause for a double exothermic peak noticeable in DSC traces at temperatures between 530 K and 650 K. In practice, however, the interpretation of the double-peak behavior observed for AA2000-series alloys

* AGH - UNIVERSITY OF SCIENCE AND TECHNOLOGY, AL. MICKIEWICZA 30, 30-611 KRAKÓW, POLAND

Corresponding author: blaz@agh.edu.pl

reported in the literature is not consistent. In the most recent report, DSC maxima observed for the AA2024 alloy at 543 K and 573 K, and a double peak recorded for the AA2324 alloy were ascribed to the development of the S1 and S2 phases [9]. Some previous experiments on the AA2024 and AA2618 alloys had also revealed a double peak in DSC traces for solution-treated samples; this double peak disappeared after preliminary ageing at 498 K/1h [3]. However, in this case a different interpretation was presented – the double peak was attributed to the development of the θ" and θ' phases, which strongly overlaps S' precipitation. In yet another report, the formation of an exothermic θ' phase that appeared between 470 K and 570 K for the AA2219 alloy (Cu 6.2wt%, Mg<0.02 wt%) was thought to be responsible for a *single* peak in the DSC curves [10, 11]. Following endothermic θ' dissolution reaction and superimposed exothermic θ-particles formation, the DSC curve leveled off at 570 K – 620 K. Finally, another report attributed a single peak observed during DSC testing of Al-2.81Cu-1.05Mg-0.41Mn (wt%) alloy preliminarily aged at 423 K/(24-72h) to the development of the *S phase* [12].

It should be kept in mind that if a sufficiently high heating rate is applied or if the sample is aged at a low temperature prior to DSC testing, a double peak may change to a single peak [3, 13].

Since the location of specific DSC peaks with respect to particular phase reactions is not the main focus of the present study, it is simply assumed that the effects for θ' and S' precipitation strongly overlap in DSC thermograms. Consequently, the total exothermic effects observed for the AA2024 alloy at temperatures ranging from 520 to 650 K, including a double exothermic peak, are denoted as the θ' + S' reaction throughout the paper.

Apart from the precipitation hardening of aluminum alloys, particular attention in technological procedures is paid to grain refining, which usually leads to additional strengthening of the material according to the commonly known Hall-Petch relation. However, structural effects related to the precipitation hardening of ultra-fine-grained materials are more complex than those observed for commercial alloys, which is why material hardening cannot be considered a simple super-positioning of mentioned processes. For example, equal channel angular pressing (ECAP) of solution-treated Al-Zn-Mg alloy was reported to result in effective grain size refining due to intense recovery of highly deformed material [14]. However, ageing of highly deformed samples did not correspond to typical precipitation sequences observed in coarse-grained industrial alloys. Instead of initial nucleation of metastable phases, i.e. G-P→η'→η particles, the heterogeneous growth of stable η particles at grain boundaries was observed. As a result, the precipitation hardening effect was negligible. Similar experiments were reported for the Al-4% Cu alloy [15]. Direct nucleation and growth of stable θ-particles (Al_2Cu) were reported for samples which were solution-treated and heavy-deformed using ECAE, and then aged at room temperature. It is worth stressing that the nucleation of fine metastable θ'' and θ' precipitates, which are commonly reported for industrial materials, was not reported. The growth of equiaxial θ-type precipitates at grain boundaries was also observed in the ultra-fine grained Al-1.7at% Cu alloy highly deformed by means of the ECAP method [16]. The development of a stable θ-phase and the enhanced growth of precipitates during artificial ageing was attributed to intense grain boundary diffusion.

Highly refined structure of materials can be produced using powder metallurgy (PM) methods, which are preceded by a powder milling (MA) procedure. For example, high-strength AA2219 material produced by means of MA/PM methods was reported to exhibit low porosity (<1%) and grain size <40nm [17]. Comparable experiments on the AA2024 MA/PM alloy lead to the conclusion that powder milling also causes a noticeable oversaturation of the solid solution; this was ascribed to the partial dissolution of some Al_2Cu precipitates [18]. During the subsequent hot consolidation procedures, the remaining particles as well as other insoluble nano-sized aluminum oxides, allowed the material to maintain a high thermal stability of its mechanical properties. This was attributed to effective grain boundary pinning by the particles, which retarded the coarsening of the grains.

During the recent years, particular attention has been paid to the utilization of scrap metal in the industrial practice and the production of composites based on light-metal matrix [19-23]. Commonly used PM procedures were proposed for the bulk material production from scrap metal in order to avoid metal loss during metallurgical procedures. It was also reported that highly-refined structure of bulk products can be received with success from scrap metal by means of MA/PM procedures that combine the milling of chips and the mechanical consolidation of as-milled powders. However, the milling parameters have to be carefully determined experimentally in order to finish the milling process and to reach the maximum strengthening of the final bulk material. Unfinished milling of components leads to the development of a bimodal structure that contains unmilled remains of chips.

Experiments on the 7N01 alloy (~AA7005) manufactured by means of MA/PM procedures were performed to show the effect of grain refinement on dynamic precipitation effects during hot compression of samples which had undergone preliminary solution treatment [19, 20]. Compression tests performed at 293 K – 773 K for commercial aluminum 7N01 alloy and very-fine grained MA/PM materials have shown that increasing milling time and the related refining of the material structure result in relatively high strength of the material over a wide range of deformation temperatures. However, the hardening of solution-treated samples, which is related to the dynamic precipitation effect, diminishes when the grain size is reduced as a result of the milling. Electron microscopy observations performed on solution-treated and hot-deformed MA/PM samples revealed negligible coarsening of preliminarily formed very fine-grained matrix. It was noticed that the majority of fine grains was comparable in size to the width of the precipitation free zone usually reported for aged industrial materials. Therefore, it was concluded that the heterogeneous precipitation at grain boundaries diminishes the alloying element content inside very fine grains. In consequence, disabled homogeneous precipitation inside the grains, which is necessary for the effective hardening, was suspended.

The afore-mentioned aspects of the precipitation processes in very fine-grained aluminum alloys require further investigation. To address this issue, differential scanning

calorimetry (DSC) tests and transmission electron microscopy (TEM) observations were performed to study the structural effects of MA/PM procedure on the precipitation processes in MA/PM AA2024 material in comparison to typical structural processes in commercial AA2024 material.

2. Experimental

The chemical composition of the tested 2024 aluminum alloy is presented in Table 1. The chips obtained by the machining of an AA2024 as-extruded bar were mechanically refined via milling in an Attritor ball mill for 8 h and 30 h. An addition of 2-3wt% of flaked graphite was used to avoid the agglomeration of powder particles. The as-milled powder was put in a container made of the 6061 alloy and compressed under 500 MPa, then vacuum-degassed for one hour under a pressure of 100 MPa.

TABLE 1

Chemical composition of the tested 2024 aluminum alloy

Element, % mass									
Si	Fe	Cu	Mn	Mg	Cr	Zn	Ti	Zr	Al
0.15	0.15	4.40	0.63	1.60	0.10	0.25	0.15	0.05	in balance

The compressed material was extruded at 673 K and rods with a diameter of 7 mm were obtained using cross-section reduction of λ=25. A lateral layer composed of the 6061 alloy was removed during the machining of cylindrical samples Ø5 mm x 1.5 mm for differential scanning calorimetry tests. For comparison purposes, a bar from the commercial AA2024 hot-extruded alloy was used to manufacture Ø7 mm rods under the same extrusion conditions. Samples prepared using the MA/PM method and those extruded from the industrial bar are henceforth referred to as 2024MA and 2024IM, respectively. Some samples (marked with *p*) were annealed at 768 K for 300 minutes, and quenched in cold water. Sample denotation, which includes milling time and heat treatment conditions, is shown in Table 2.

TABLE 2

Sample denotations

Denotation	Extruded material	Sample treatment
2024IM	Commercial alloy	As extruded
2024IMp		Solution-treated at 768 K/300 min
2024MA8	Chips milled for 8 hours	As extruded
2024MA8p		Solution-treated at 768 K/300 min
2024MA30	Chips milled for 30 hours	As extruded
2024MA30p		Solution-treated at 768 K/300 min

Differential scanning calorimetry (DSC) tests were performed using the Mettler Toledo DSC822e device and an argon protective atmosphere. DSC curves were recorded for samples heated up to 768 K at a constant heating rate of 20 K/min. The recorded DSC curves were then analyzed to determine the specific temperature of exothermic peaks and the related heat energy values, DH. The DH energy corresponding to the exothermic peak area was determined by cutting the peak area above the base line, which was estimated according to the computer program installed on the Toledo device and arbitrarily selected start/finish temperatures for the peak appearance.

X-ray diffraction phase analyses (XRD) were performed using the Rigaku Miniflex II equipment. Prior to XRD analysis, the samples were annealed at 768 K/ 300 min (495°C), and slowly cooled inside the furnace. The as-received sample was mechanically powdered, after which XRD analyses were performed using CuK_α rays and 2Θ angle over the range of 30° – 100°.

3. Results

3.1. Calorimetric tests

Calorimetric tests were performed on both solution-treated and as-extruded samples to examine the effect of the preliminary milling procedure on DSC characteristics and the related structural processes in highly refined material. The DSC curves recorded for IM and MA/PM samples are shown in Fig. 1.

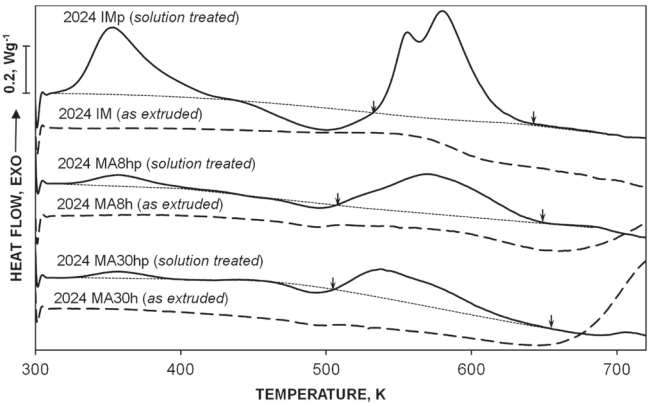

Fig. 1. DSC curves for both as-extruded and solution-treated IM and MA samples. The values of the released heat, DH, which correspond to θ'+S' precipitation peaks, are listed in Table 3

TABLE 3

Characteristic temperature of θ'+S' precipitation peak for solution-treated 2024IMp, 2024MA8p and 2024MA30p samples

Sample	Heat energy emitted J/g	Characteristic temperatures of θ'+S' precipitation start and exothermic peak maximum development	
		start	peak maximum
2024IMp	33.5	535 K	558 K and 583 K
2024MA8p	17.3	510 K	567 K
2024MA30p	13.8	505 K	548 K

According to literature data, it was assumed that the first maximum observed on the DSC curves at 350-410 K for solution-treated IM material resulted from the development of G-P-B zones. The following endothermic effect at ~500 K is commonly attributed to dissolving G-P-B zones that precede the nucleation of θ'' and/or S'' metastable particles [11, 12]. The subsequent enhanced exothermic effects at

500 K – 650 K are ascribed to the precipitation of dispersive θ'' and θ' or S' and S particles; the predominance of either the former or the latter type of particles depends on the Cu:Mg ratio. High dispersion of the particles is commonly believed to result in the maximum hardening of the material, while the subsequent softening effect is ascribed to particle coarsening [3, 13].

The double peak revealed for the 2024IMp sample (540 K - 640 K) was found to turn into a single peak and to spread along the temperature axis for 2024MA8p and 2024MA30p samples. The calculated values of energy, which are related to the total exothermic effect, and the characteristic temperatures for the peak start are given in Table 3.

Precipitation effects did not occur in the as-extruded samples. That is why only a slightly-marked endothermic effect related to particle dissolution was detected at 550 K - 650 K. For higher temperatures, i.e. above ~650 K, an exothermic effect was detected for as-extruded MA/PM materials; this effect was not observed on the DSC curves recorded for the as-extruded IM sample.

3.2. XRD phase analysis

XRD phase analysis results received for both IM and MA/PM materials annealed at 768 K/300 min and slowly cooled in the furnace revealed characteristic peaks ascribed to specific phases formed in particular materials (Fig. 2). The peaks related to the equilibrium θ-phase (Al_2Cu) as well as slightly marked peaks of S-phase (Al_2CuMg) were observed for the industrial over-aged material. XRD tests on MA/PM materials revealed peaks corresponding to the Al_2Cu crystal lattice and clearly marked peaks for aluminum carbide (Al_4C_3). The peaks originating from the S-phase were practically not detected on the XRD diagrams received from the milled materials.

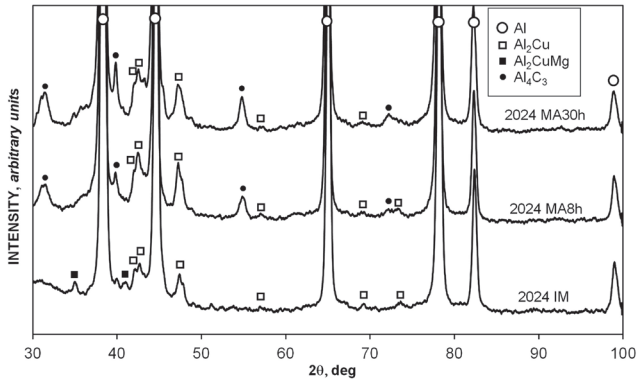

Fig. 2. X-ray diffraction phase analysis results for 2024IM and 2024MA8h and 2024MA30h samples annealed at 768 K/300 min and slowly cooled in the furnace

3.3. Structural observations

Optical microscopy observations of as-extruded materials revealed material with highly refined structure interspersed between residues of non-refined chips. Light areas (C) observed in the material structure correspond to the unrefined residues of chips (Fig. 3a-b). Relatively dark areas (M) of heavily refined structure were found to dominate with prolonged milling time. Detailed structural observations and chemical analysis of components were performed using TEM/EDS methods. Thin foils were prepared via mechanical grinding with fine abrasive papers and finally polished by means of the ion thinning method. The typical TEM microstructures of the material extruded after 8 and 30 hours of milling are shown in Fig. 4a and Fig. 4b, respectively. Specific structural components of the material, i.e. chip residues (C) and heavily milled parts (M), are marked in the figure.

TEM/STEM structural observations and chemical analysis of fine components were also performed for samples heated in the calorimeter at a constant heating rate. DSC curves allowed the assessment of the approximate start and finish temperature of the precipitation range. Thus, solution-treated samples were heated in the calorimeter to finish the ageing process, and then immediately quenched in water. Samples were heated to the following temperatures: 2024IM – 585 K, 2024MA8 - 640 K, 2024MA30 – 620 K. Structural observations of the 2024IM sample heated to 585 K revealed commonly observed disc-shaped θ' / S' particles on {100}Al planes and relatively coarse Cu-rich precipitates that nucleated heterogeneously at grain boundaries (Fig. 5). Heterogeneous precipitation and growth of coarse Cu-rich precipitates on pre-existing Mn-rich particles (presumably Al_6Mn) and on other pre-existing (Fe, Mn, Cr)-rich particles was also observed (Fig. 5a). Consequently, EDX analysis of these relatively coarse particles, marked A-E in Fig. 5a, revealed element composition which did not correspond to a single, specific phase, but instead to the average composition of particle agglomerates (Table 4).

TABLE 4
EDX analysis results obtained for particles marked A-F in Fig. 5

% mass	Mg	Al	Cr	Mn	Fe	Cu	Zn
A	1.5	83.0		6.7		8.8	
B	2.4	78.0		8.3	0.3	11.0	
C	3.9	72.1	0.2	8.1	0.4	15.3	
D		76.8		2.0	3.7	17.5	
E		79.6		1.8	3.7	14.9	
F (matrix)		97.1		0.2		2.5	0.2

As mentioned previously, the most characteristic feature of the as-milled MA/PM material is related to its bimodal structure containing highly refined structural components and residues of unmilled grains. In spite of high temperature and prolonged annealing time (768 K/300 min), the refined areas of the structure (M) apparently remained (Fig. 6a). SAD analysis of heavily refined M-area revealed diffraction rings, which are characteristic for very fine-grained material (Fig. 6b). In spite of Al-diffraction rings, some fine diffraction rings were found to fit the Al_4C_3 structure. An enlarged dark field image of the M-area, received from the {012}Al_4C_3 diffraction ring, is shown in Fig. 6c. Bright nano-sized Al_4C_3 particles are marked in this figure.

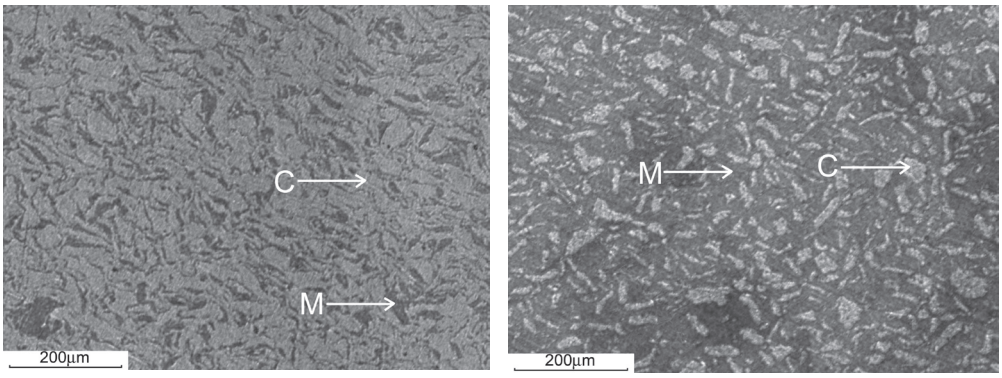

(a) (b)

Fig. 3. Microstructure of MA/PM-processed and hot-extruded material received after a milling time of: a) 8 hours; b) 30 hours (optical microscopy; C – chip residue, M – heavy refined microstructure)

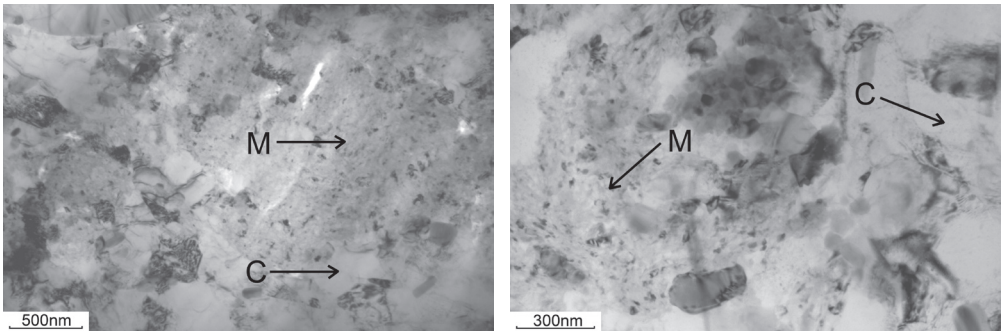

(a) (b)

Fig. 4. TEM microstructure of MA/PM-processed and hot-extruded 2024 alloy received after a milling time of: a) 8 hours; b) 30 hours (C – chip residue, M – heavy refined microstructure)

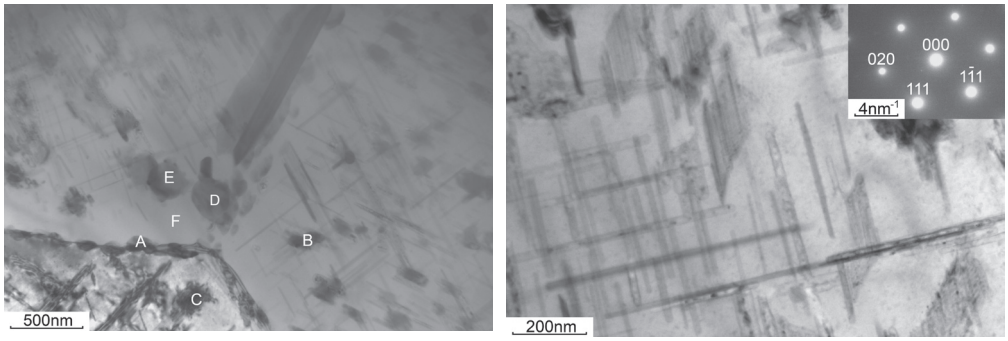

(a) (b)

Fig. 5. TEM microstructure of the 2024IM sample solution-treated at 768 K/ 300 min and then heated in the calorimeter up to 585 K at a constant heating rate: a) near-grain boundary area (EDX chemical analysis results for particles marked A-E are shown in Table 4); b) characteristic distribution of semicoherent θ'/S'-type plates on {001}Al planes (inset SAD pattern obtained from the matrix)

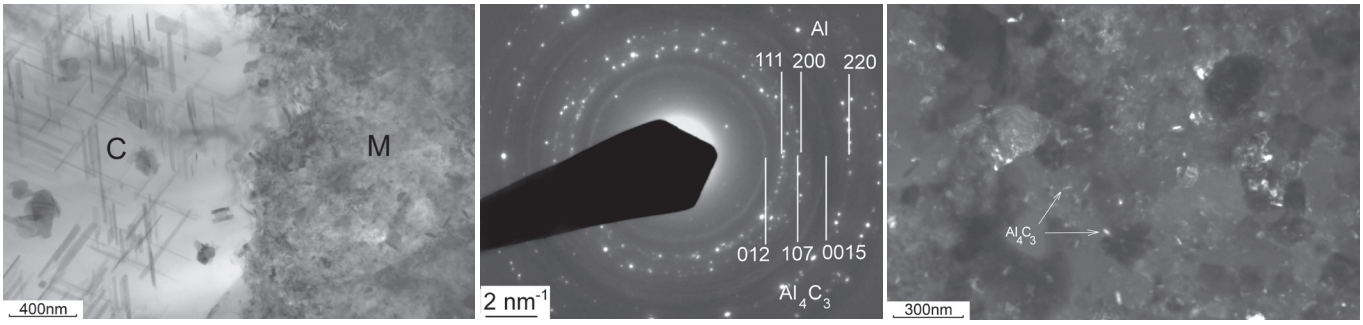

(a) (b) (c)

Fig. 6. TEM microstructure of the 2024MA8h sample solution-treated at 768 K/ 300 min and then heated in the calorimeter up to 640 K using a constant heating rate: a) TEM image; b) SAD pattern received from M-area; d) dark field image received from {012}Al_4C_3 diffraction ring

It was impossible to analyze the majority of the finest structural components via STEM element mapping due to the relatively low resolution of this method (Fig. 7). However, some noticeable differences in the morphology of relatively coarse Cu-rich particles were revealed. The coarsening of Cu-rich particles during ageing (presumably the Al_2Cu phase) was found to be more effective in the M-area (left-upper corner) than in the C-area with unmilled grains. Oxygen distribution map was omitted as no noticeable difference in the element distribution was detected.

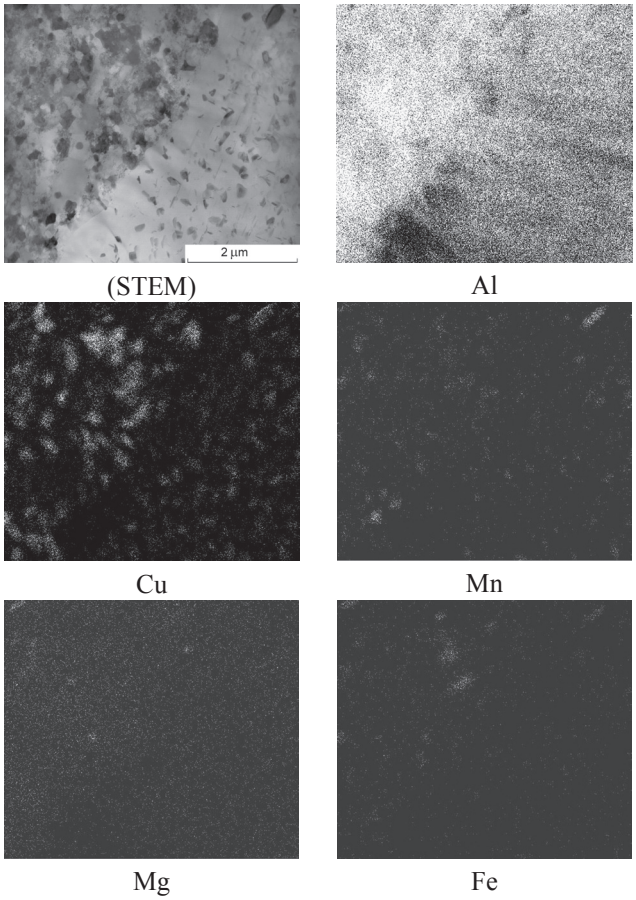

Fig. 7. STEM element mapping for the 2024MA30hp sample heated up to 618 K at the constant heating rate of 20K/min

4. Discussion

The mechanical processing of metallic chips, which includes milling in a protective atmosphere as well as the subsequent pressing, vacuum degassing and hot extrusion processes, was found to be a prospective method for the production of nano-grained bulk materials. However, to obtain a material with the most desirable properties, it is crucial to determine the optimum values of the most essential parameters, which include primarily milling intensity and milling time.

The milling parameters which had been elaborated experimentally for the production of mechanically alloyed composites and other PM materials [17, 24-26] were found to be insufficient for the refining of relatively coarse AA2024 chips. Even when a milling time of 30 hours was applied, structural observations revealed the development of bimodal-type of the MA/PM material structure that was composed of unrefined chip's residues incorporated between highly-refined structural components, which are marked as M and C, respectively (Fig. 3 and Fig. 4). The specific volume of the refined structure (M) was found to increase from 27 vol. % to 73 vol. % for the material milled for 8 h and 30 h, respectively.

Particular attention was paid to the assessment of the effect of grain refinement on the structural processes occurring the in AA2024 alloy. First, differential scanning calorimetry tests were performed for both as-extruded materials and the samples solution-treated at 768 K/300min. The recorded DSC curves did not reveal any exothermic peaks related to the ageing process for the as-extruded materials. It was concluded that the monotonic decrease of the DSC curve at 500 K – 650 K can be ascribed to the dissolution of q and S particles, which are commonly observed in hot-extruded commercial AA2024 materials. Heating as-extruded 2024MA8h and 2024MA30h samples revealed exothermic effects above ~650 K, which can be attributed to the supplementary recovery effect for heavy-deformed material formerly extruded at 673 K. The additional input to the heat release above ~650 K can be attributed to the chemical reaction between the aluminum matrix and carbon (graphite flakes), which yields Al_4C_3 particles (Fig. 6b-c).

Experiments were also performed on the solution-treated samples to test the effect of the material structure refinement on consecutive structural processes induced by the solution treatment and ageing procedures. It is worth stressing that the solution treatment at 768 K/300 min did not result in noticeable grain coarsening of the heavy-refined structure. Even the very fine structure observed in the M-area survived in spite of high-temperature heat treatment and the subsequent heating of the sample in the calorimeter (Fig. 6). These results confirm that grain boundary pinning by nano-sized (AlMg)-oxides and Al_4C_3 particles as well as other insoluble precipitates effectively retards the grain coarsening.

The refining of the material structure through MA/PM processing was found to result in effective reduction of the peak related to G-P-B zones, which typically develops at ~350 K. Both G-P-B zones and nucleation of metastable θ'' particles are commonly reported for initial steps of ageing in coarse-grained commercial alloys. However, the volume of coarse-grained chip residues in the tested 2024MA8 and 2024MA30 materials is reduced with increased milling time. In consequence, the volume of very fine metastable phases nucleating in the grain interior diminishes.

As mentioned previously, a double exothermic peak above ~470 K on the DSC curve for 2024IMp sample (Fig. 1) coincides with the precipitation heat effects, which are observed for other industrial AA2000 series alloys containing an Mg addition [3, 13]. DSC tests performed on solution-treated 2024MA8p and 2024MA30p samples point to relatively effective precipitation and growth of particles in solution-treated MA/PM materials. The exothermic peak of θ' + S' precipitation shifts to lower temperature with respect to that observed for 2024IMp sample (Fig. 1). Moreover, the double peak is transformed to a single peak for fine-grained MA/PM samples; moreover, the single peak becomes evidently diffused along the temperature axis. The last effect can be ascribed to different intensities of the precipitation process in C and M areas.

The most significant conclusion is related to the effect of milling time on the heat energy, i.e. ΔH, which is released as

a result of the precipitation of θ' or θ' + S' phases. The value of ΔH is clearly reduced with increased milling time. Moreover, the double peak recorded for the solution-treated IM sample is transformed into a single peak that spreads along the temperature axis with increased milling time of MA samples. The heat effect resulting from the precipitation of θ' + S' particles in commercial 2024 aluminum alloy was reported to reach ΔH=30-33 J/g [3]. This is very close to ΔH= 33.5 J/g received for the already tested 2024IMp sample (Table 3). The double peak for the commercial AA2024 was also observed at very similar temperatures, i.e. 559K and 579K, with respect to 558K and 583K for 2024IMp sample. Relatively low ΔH values of 17.3 J/g and 13.8 J/g were observed for very fine-grained 2024MA8p and 2024MA30p samples, respectively. Badini et al. [3] also reported a reduced value of ΔH (19 J/g) and reduced temperature of a single peak maximum (551 K) for fine-grained AA2024+SiC composite; they attributed this to the precipitation of metastable (θ'' + θ' + S') phases. However, the expected effects of the particles heterogeneous nucleation at SiC/Al-Cu interphases and grain boundaries in moderately fine-grained structure of the composite were not discussed.

The relatively low ΔH values observed for the tested 2024MA8p and 2024MA30p materials may result from reduced specific volumes of the phases that form in very-fine grained material. This is consistent with high-resolution TEM/EDX investigations reported in the literature, which confirm the increased solubility of Mg, Cu at grain boundaries in highly refined aluminum alloys [27-29]. Experiments performed on some other nanostructured AA2000 series alloys also confirm the conclusion on the reduced volumes of the Al_2Cu precipitates which develop due to ageing compared to the volume of precipitates in aged commercial material [18, 30, 31]. It is worth mentioning that inconsistent results were reported for Zn distribution at grain boundaries. Liddicoat et al. [27] (2009) have found that 39% of Zn, Mg solutes in the 7075 alloy is involved in atomic clustering and most of this is allocated to the modal clusters composed of 8-12 atoms, which concentrate in particular at some grain boundaries and boundary triple points. However, more recent investigations presented by G. Sha et al. [29] (2011) lead to the opposite conclusion, namely that grain boundaries are deprived of Zn-solutes.

The most effective suppression of very-fine metastable phases' precipitation in aluminum alloys is reported for solution-treated alloys subjected to severe plastic deformation (SPD) before the ageing of the material [14-16, 18]. It was shown that direct growth of θ-type particles occurs at room temperature if the solution-treated Al-4%Cu alloy had been heavy-deformed by means of the SPD method [15]. Moreover, no evidence of metastable phases' development was found.

A similar enhancement of θ-type particle coarsening was reported if the development of localized flow and shear bands (SB) preceded static or dynamic precipitation in AA7000 and AA2000 series aluminum alloys [32-34]. It was suggested that intense coarsening of precipitates might be ascribed to privileged nucleation of particles at dense dislocation walls of SBs as well as an enhanced core diffusion mechanism at dislocation tangles.

Structural observations of heat-treated 2024MA8hp and 2024MA30hp materials lead to the general conclusion on the remarkably high stability of the bimodal structure during annealing at high temperature. Grain coarsening in heavily refined M-areas was almost entirely inhibited and structural effects of the recovery process were negligible during solution treatment at 768 K/300 min. This can be attributed to the pinning of grain boundaries by highly dispersed Al/Mg-oxides, fine Al_4C_3 particles, and other insoluble phases. Very fine aluminum oxide plates are formed on MA powder particles and fine aluminum carbide particles can grow during annealing. Unfortunately, both STEM/EDS and TEM/SAD pattern analyses of highly refined particles in the M-area were not fully successful because of the nanometric size of mixed components. The diffraction rings observed on the SAD pattern, which are shown in Fig. 6b, confirmed the development of very fine- grained aluminum matrix and nano-sized Al_4C_3 particles. As previously mentioned, Al4C3 particles formed due to the chemical reaction between the Al-matrix and the graphite flakes, a small amount of which was used as a process control agent during the milling of chips [35]. The dark field image shown in Fig. 6c was received using an electron beam swept to the $\{012\}Al_4C_3$ diffraction ring. This way, very fine Al_4C_3 grains could be distinguished on the dark background of the image. Other diffraction spots, observed between mentioned diffraction rings, can result from q-phase particles. However, the detection of specific diffraction spots, which might confirm θ or S-structure of Cu-rich particles in the M-area, failed. It is worth noting that relatively coarse Cu-rich particles, presumably θ-type, were detected using STEM element mapping (see: left-upper part of Cu-distribution map in Fig. 7). The morphology of the θ' particles in the C-area of aged MA-materials (Fig. 7a) is similar to that observed for the 2024IMp sample heated to 585 K (Fig. 5).

STEM and element mapping results lead to the conclusion on the facilitated coarsening of particles within the heavily refined area of the material structure. This effect can result from the high density of preferred nucleation sites at grain boundaries. Additional input to the enhanced growth of particles can be delivered by an efficient diffusion along the boundaries that is multiplied by the high specific grain boundary area in the M-structure.

Moreover, it seems reasonable to expect that magnesium content in the Al-matrix was depressed due to the magnesium's high affinity for oxygen. The diffusion of magnesium to the surface of milled powder granules can result in the development of complex aluminum-magnesium oxides [24-26]. In the case of milled chips of the AA2024 alloy, the reduction of Mg in the solid solution can be responsible for depressed nucleation of S-type precipitates in aged 2024MA8hp and 2024MA30hp samples. This conclusion is consistent with XRD and DSC results (Fig. 1 and Fig. 2). Characteristic peaks originating from the S-structure, which are slightly marked in XRD spectrum for the 2024IMp sample (Fig. 2), disappear entirely for the 2024MA8hp and 2024MA30hp materials.

5. Conclusions

1. Combined milling of AA2024 chips and mechanical consolidation of as-received powders via pressing, vacuum degassing and hot extrusion is a prospective method for the manufacture of bulk material with very

fine-grained structure.

2. A milling time of 30h was not sufficient to finish the refinement of milled chips. Structural observations of the as-extruded 2024MA8h and 2024MA30h materials revealed 73% and 27% of unmilled residue content, respectively. In spite of solution treatment at 768 K/300 min, highly refined components of the structure remained.
3. DSC tests performed on the solution-treated 2024MA8hp and 2024MA30hp samples revealed a noticeable reduction in the temperature at which the exothermic peak of θ' + S' precipitation was recorded. This was ascribed to enhanced diffusion within the highly refined structure of milled material and a relatively easy heterogeneous nucleation and growth of the particles at grain boundaries.
4. Due to the magnesium's high affinity for oxygen, the development of a thin oxide layer on milled powders was assumed to reduce magnesium content inside very fine Al-matrix grains. As a result, the nucleation of S' particles in milled materials was depressed.
5. Heat effects were reduced with increased milling time for both G-P-B zones and θ' + S' phase growth. The diminishing exothermic θ' + S' precipitation peak was attributed to the increasing solubility of solutes in the highly refined structure of the alloy.
6. Adding graphite as a process control agent to protect mechanical bonding of milled powders results in the development of fine Al_4C_3 particles in 2024MA8hp and 2024MA30hp materials. The particles form at high temperature due to the chemical reaction between the Al-matrix and the fine graphite flakes.

Acknowledgements

The authors are very grateful to Prof. Makoto Sugamata and Prof. Junichi Kaneko for their contribution to the research program and our co-workers at the Nihon University lab for the manufacture of tested materials. Financial support from the National Science Centre, grant No: 2011/01/B/ST8/03012, is kindly acknowledged.

REFERENCES:

[1] G. Sha, R.K.W. Marcelu, X. Gao, B. C. Muddle, S.P. Singer, Acta Mater. **59**, 1659-1670 (2011).
[2] D.J. Chakrabarti, D.E. Laughlin, Prog. Mater. Sci. **49**, 389-410 (2004).
[3] C. Badini, F. Marino, E. Verne, Mater. Sci. Eng. A**191**, 185-191 (1995).
[4] H.K. Hardy, J. Inst. Met. **83**, 17-34 (1954-55).
[5] S.P. Ringer, K. Hono: Mater. Characterization 44, 101-131 (2000).
[6] S.M. Kumaran, Mater. Sci. Engr. A**528**, 4152-4158 (2011).
[7] S.C. Wang, M. J. Starink: Acta Mater. 55, 933-941 (2007).
[8] C.H. Gür, I. Yildiz, Proc. 16-th World Conf. NDT, Montreal, Canada, (2004).
[9] J.M. Papazian, Metall. Trans. A **12.2**, 269-280 (1981).
[10] J. M. Papazian, Metall. Trans. A **13.5**, 761-769 (1982).
[11] S. C. Wang, M. J. Starink, Intern. Mater. Rev. **50**, 193-215 (2005).
[12] S. Muthu Kumaran, J. Alloys Compd **539**, 179-183 (2012).
[13] J. Gubicza, I. Schiller, N.Q. Chinh, J. Illy, Z. Horita, T.G. Langdon, Mater. Sci. Eng. A **460–461**, 77-85 (2007).
[14] Y. Huang, J. D. Robson, P. B. Prangnel, Acta Mater. **58**, 1643-1657 (2010).
[15] M. Muraymama, Z. Horita, K. Hono, Acta Mater. 49, 21-29 (2001).
[16] T. Shanmugasundaram, V. Subramanya Sarma, B. S.Murty, M. Heilmaier, Mater. Sci. Forum 584, 97-101 (2008).
[17] L. Guoxian , L. Zhichao, W. Erde, W. Zhongren, J. Mater. Proc. Tech. **58**, 247-250 (1996).
[18] J. Koziel, L. Blaz, A. Kula, M. Sugamata, G. Wloch, Structure and properties of fine-grained aluminum alloy 7000 serie – 11-th Intern. Conf. TECHNOLOGY2009 – Bratislava 9 – 10 September 2009 (CD, electronic edition of the Conference Proceedings).
[19] A. Kula, L. Blaz, J. Koziel, M. Sugamata, G. Wloch, Intern. Conf. Engineering and Education 2008 – Białka Tatrzańska, 63-68 (2008).
[20] Kim, Deung Gyu, J. Kaneko, M. Sugamata, JIM, Mater. Trans. **36**, 305-311 (1995).
[21] Kula, L. Blaz, J. Kaneko, M. Sugamata, J. Micr. **237**, 421-426 (2010).
[22] M. Sugamata, K. Shiina, M. Kubota, J. Kaneko, J. Alloys Compd. 483, 350-354 (2009).
[23] L. Blaz, J. Kaneko, M. Sugamata, Z. Sierpinski, M. Tumidajewicz, Mater. Sci. Tech. **20**, 1639-1644 (2004).
[24] L. Blaz, J. Kaneko, M. Sugamata, Z. Sierpinski, M. Tumidajewicz, Mater. Sci. Tech. **21**, 715-721 (2005).
[25] K. Seimiya, M. Sugamata, L. Blaz, J. Kaneko, J. Jpn. Soc. Powder and Powder Metallurgy **53**, 899-908 (2006).
[26] P.V. Liddicoat, Xiao-Zhou Liao, S. P. Ringer, Mater. Sci. Forum **618-619**, 543-546 (2009).
[27] N.A. Enikeev, M. Yu. Murashkin, X. Sauvage, V.U. Kazykhanov, R. Z. Valiev, Mater. Sci. Forum **667**, 665-669 (2011).
[28] G. Sha, L. Yao, X. Liao, S. P. Ringer, Z. C. Duan, T.G. Langdon, Ultramicroscopy **111**, 500-505 (2011).
[29] T. Shanmugasundaram, M. Heilmaier, V. S. Sarma, B.S. Murty, Mater. Sci. Forum **690**, 234-237 (2011).
[30] T. Shanmugasundaram, V. S. Subramanya, B.S. Murty, M. Heilmaier, Mater. Sci. Forum **584**, 97-101 (2008).
[31] K. Piela, L. Blaz, Z. Sierpinski, T. Forys, Arch. Metall. Mater. **57**, 704-709 (2012).
[32] L. Blaz, K. Piela, Mater. Sci. Tech. **23**, 1-7 (2007).
[33] O. Woznicka, L. Blaz, E. Evangelista, J. Alloys Compd. **378**, 339-342 (2004).
[34] H. Arik, Mater. Design **25**, 31-40 (2004).

Received: 20 February 2015.